



Electric Field- and Temperature-Induced Phase Transitions in High-Strain Relaxor-Based Ferroelectric $\text{Pb}(\text{Mg}_{1/3}\text{Nb}_{2/3})_{1-x}\text{Ti}_x\text{O}_3$ Single Crystals

Authors: R. R. Chien , V. Hugo Schmidt , C.-S. Tu , F.-T. Wang , I.-C. Shih , L.-W. Hung & H. Luo

This is an Accepted Manuscript of an article published in [Ferroelectrics](#) on December 7, 2007, available online: <http://www.tandfonline.com/10.1080/00150190701515055>.

R. R. Chien , V. Hugo Schmidt , C.-S. Tu , F.-T. Wang , I.-C. Shih , L.-W. Hung & H. Luo (2007) Electric Field- and Temperature-Induced Phase Transitions in High-Strain Relaxor-Based Ferroelectric $\text{Pb}(\text{Mg}_{1/3}\text{Nb}_{2/3})_{1-x}\text{Ti}_x\text{O}_3$ Single Crystals, *Ferroelectrics*, 359:1, 99-110, DOI: 10.1080/00150190701515055

Made available through Montana State University's [ScholarWorks](#) scholarworks.montana.edu

Electric Field- and Temperature-Induced Phase Transitions in High-Strain Relaxor-Based Ferroelectric $\text{Pb}(\text{Mg}_{1/3}\text{Nb}_{2/3})_{1-x}\text{Ti}_x\text{O}_3$ Single Crystals

R. R. CHIEN,^{1,*} V. HUGO SCHMIDT,¹ C.-S. TU,² F.-T. WANG,²
I.-C. SHIH,³ L.-W. HUNG,³ AND H. LUO⁴

¹Department of Physics, Montana State University, Bozeman, MT 59717, USA

²Graduate Institute of Applied Science and Engineering, Catholic Univ., Taipei 242, Taiwan, R.O.C.

³Department of Physics, Fu Jen Catholic Univ., Taipei 242, Taiwan, R.O.C.

⁴Shanghai Institute of Ceramics, Chinese Academy of Sciences, Shanghai 201800, People's Republic of China

As a review, we compare results in electric-field- and temperature-induced phase transitions for four $\text{Pb}(\text{Mg}_{1/3}\text{Nb}_{2/3})_{1-x}\text{Ti}_x\text{O}_3$ (PMNT- x) single crystals, namely (001)-cut PMNT- x ($x = 24\%$, 33% , and 40%) and (111)-cut PMNT- 33% . Dielectric properties and domain states were measured as functions of temperature and electric field. The hysteresis loops of polarization versus electric field at room temperature were also measured. The intermediate monoclinic phases are essential in bridging higher symmetries while the electric-field- or temperature-induced transitions are taking place. Whether or not a monodomain state can be induced by a dc electric field strongly depends on crystallographic orientation, PbTiO_3 content, and temperature.

Keywords PMNT single crystal; dielectric permittivity; domain structure; phase transition

Introduction

Relaxor-based ferroelectric single crystals $\text{Pb}(\text{Mg}_{1/3}\text{Nb}_{2/3})_{1-x}\text{Ti}_x\text{O}_3$ (PMNT- x) and $\text{Pb}(\text{Zn}_{1/3}\text{Nb}_{2/3})_{1-x}\text{Ti}_x\text{O}_3$ (PZNT- x) have attracted much attention due to their high performance in piezoelectric related applications. These crystals with compounds near a morphotropic phase boundary (MPB) between rhombohedral (R) and tetragonal (T) phases exhibit piezoelectric properties about ten times better than the ceramics that are generally used, such as extremely large electromechanical coupling factor k_{33} ($>94\%$), ultrahigh piezoelectric coefficients (>2500 pC/N), a large strain level (up to $\sim 1.7\%$), and low hysteresis [1–4].

The relaxor ferroelectric PMNT- x is a solid solution between a complex perovskite $\text{Pb}(\text{Mg}_{1/3}\text{Nb}_{2/3})\text{O}_3$ (PMN), namely relaxor, and a simple perovskite PbTiO_3 (PT), namely

ferroelectric. Relaxors are characterized by a diffuse phase transition with frequency dispersion of the temperature giving maximum permittivity. Relaxors have disordered polarization, with small ordered polar nanoregions (PNRs) that begin to develop locally below Burns temperature (~ 620 K in PMN). In PMN, the volume fraction of the PNRs increases as the temperature decreases and reaches the three-dimensional percolation threshold below $T \sim 200$ K [5]. The PT crystal exhibits a normal ferroelectric phase transition at 490°C . Ferroelectrics have a net spontaneous polarization due to the average off-centered displacements of the atoms. The polarization can be switched in direction by an external electric (E) field, which is displayed in a hysteresis loop measurement of polarization versus E .

The piezoelectric performance of ferroelectrics arises from the interaction of the polarization and E field, i.e. the coupling of the polarization and strain. Therefore, an E field poling is usually performed on these materials to enhance piezoelectric performance before application. The very large electromechanical coupling is attributed to polarization rotation effect induced by an external dc E field between T and R phases through intermediate monoclinic (M) or orthorhombic (O) symmetries [6]. This has generated a great interest in investigating phase (structural) transitions near the MPB under the application of thermal, E field, and stress for understanding the underlying mechanism of the piezoelectric properties [7, 8].

Physical properties of PMNT- x depend strongly on titanium content, crystallographic orientation, strength of external poling E field, and temperature [7–9]. In order to understand the physical origin of the E field- and temperature-induced phase transitions, here we compare results for four PMNT- x single crystals with various titanium content and crystallographic orientation, i.e. (001)-cut PMNT- x ($x = 24\%$, 33% , 40%) and (111)-cut PMNT- 33% crystals. Hereafter, (001) PMNT- x stands for (001)-cut PMNT- x . The E field- and temperature-induced phase transitions in the single crystals are investigated by dielectric permittivity, domain observations with polarizing light microscopy, and the hysteresis loops of polarization vs. E field at room temperature (RT). By using relations of crystallographic symmetry and optical extinction, polarizing light microscopy provides a real-time direct observation of the polarization orientations in ferroelectric domains and their corresponding crystal phases.

Experimental Procedure

The four lead magnesium niobate-lead titanate crystals PMNT- x were grown using a modified Bridgman method and are cut perpendicular to a $\langle 001 \rangle$ direction for the three (001)-cut crystals, and a $\langle 111 \rangle$ direction for the (111)PMNT- 33% crystal after aligning by x-ray diffraction. The samples were cut in rectangular shape as shown in Figure 1a. The Ti concentration ($x\%$) was determined by $x = [T_m(^{\circ}\text{C}) + 10]/5$, where T_m is the dielectric maximum temperature obtained upon heating at measuring frequency $f = 10$ kHz without E field poling. Before any measurement described below, the samples were annealed in the cubic (C) phase. For dielectric measurements, a Wayne-Kerr Precision Analyzer PMA3260A with four-lead connections was used to obtain real (ϵ') and imaginary (ϵ'') parts of dielectric permittivity. A Janis CCS-450 cold-head was used with a Lakeshore 340 temperature controller. Gold film electrodes were deposited by dc sputtering on sample surfaces as shown in Figure 1a. Several different processes were used in the dielectric measurements. The first is called “zero-field-heated” (ZFH) and “zero-field-cooled” (ZFC), in which the data are taken upon heating and cooling respectively without any E field poling. The second process is

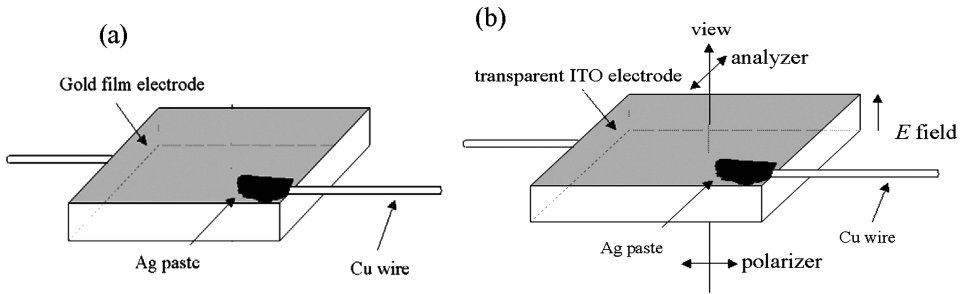


Figure 1. Sample configurations for (a) dielectric measurement and (b) domain observation under polarizing microscope.

called “field-cooled-zero-field-heated”(FC-ZFH), in which the sample is first cooled from the C phase down to RT with an E field, then cooled to 100 or 150 K without field before ZFH is performed. In the third process FR-ZFH, the sample is directly poled by an external E field for at least an hour at RT. Then the E field is removed before ZFH is performed from 100 or 150 K. In this review, we only display dielectric results from ZFH and ZFC processes. The results from other processes can be found in Refs. [7, 10-14]. The hysteresis loops of polarization vs. E field were taken at RT by using a Sawyer-Tower circuit at $f = 46$ Hz.

The domain observations as functions of temperature and E field were made by using a Linkam THMS600 heating/cooling stage mounted on a Nikon E600POL polarizing microscope with a $0^\circ/90^\circ$ crossed polarizer/analyzer (P/A) pair. The detailed experimental configuration is shown in Figure 1b. To avoid domain overlapping, the samples were polished to the thickness of about 45, 65, 45, and 50 μm for (001) PMNT-24%, (001) PMNT-33%, (001) PMNT-40%, and (111) PMNT-33%, respectively. Transparent conductive films of indium tin oxide (ITO) were deposited on the polished (001) surfaces of (001) PMNT- x samples and (111) surfaces of (111)PMNT-33% sample by dc sputtering. The edge orientations of the samples were determined by x-ray diffraction. In domain measurement, we aligned one of the sample edges with one of the crossed P/A: 0° axes so that the extinction angles shown in all domain micrographs were measured from either $\langle 110 \rangle$ or $\langle 100 \rangle$ as indicated in Figures of polarizing light micrographs. In E -field-dependent measurements, a dc E field was applied along $[001]$ for the (001) PMNT- x samples and $[111]$ for the (111) PMNT-33% sample, respectively.

Principle of Polarizing Microscopy

Various crystallographic symmetries (or phases) can be determined for most cases by measuring optical extinction angles from polarizing microscopy. For interpreting domain structures obtained from polarizing microscopy, more details of the principles of optical extinction for the (001)-cut and (111)-cut crystals can be found in Refs. [10] and [15], respectively.

Figure 2a shows the (001)-cut projection with all four sides folded out. The inner square outlines the front face of the cube. Figure 2b shows the (111)-cut projection, in which any extinctions at angles other than 0° , 30° , 60° , etc. must be from M or possibly triclinic (Tri) domains. Our observation of extinctions at such other angles is interpreted by us as indicating M domains at intermediate temperatures as discussed below.

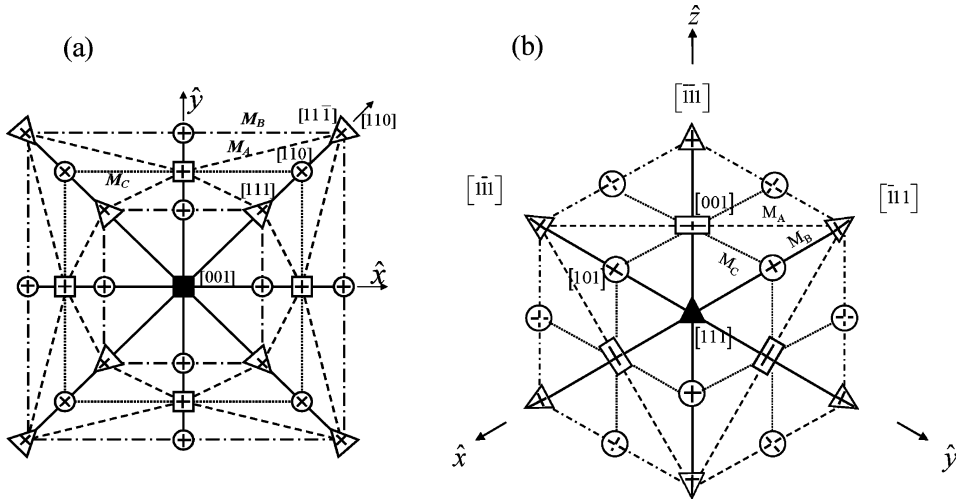


Figure 2. Relation between the optical extinction orientations corresponding to the ferroelectric polarization directions for various phases and domains projected on (a) the (001) plane and (b) the (111) plane. Dashed, dash-dotted, and dotted lines represent polarization directions for M_A -, M_B -, and M_C -type monoclinic phase domains, respectively.

To determine the crystal phase (symmetry) from measuring the extinction angles with the extinction patterns of Fig. 2, we aligned one of the crossed P/A pair axes at reading 0° with one sample edge, such as [110] or [100]. The extinction angles therefore are measured with respect to the [110] or the [100] directions. The solid crosses within the symbols in Figure 2 represent the orientation of the extinction. For instance, if the (001)-cut sample's [110] edge is aligned with P/A: 0° , R phase domains represented by triangles with solid crosses thus have extinction at 0° (or 90°) as shown in Fig. 2a. T phase domains represented by squares with solid crosses have extinction at 45° . T phase domains with polarization P along the [001] axis represented by the solid black square in the center have extinction at every orientation of the crossed P/A pair and are written as “T₀₀₁” in the following discussion. The O phase domains represented by circles with solid crosses have extinctions at 0° (or 90°) or 45° , whereas R domains only give extinctions at 0° . Thus, the (001)-cut shown in Figure 2a clearly distinguishes R from T phases by the 45° extinction angle difference. Any extinctions at angles other than 0° (or 90°) and 45° must be from the M or Tri phase domains. Note that all the phases except Tri phase have been reported in various PMNT crystals. Our large observed variation in extinction angle with E field or temperature indicates M domains whose polarization P can vary with E field through a large angle, whereas the polarization directions are nearly fixed for R, T, or O domains as E field or temperature varies.

Results and Discussion

Figure 3 shows the temperature-dependent and frequency-dependent dielectric permittivity measured in the four unpoled crystals. In (001)PMNT-24% (Fig. 3), $\epsilon'(T)$ was found to follow the Curie-Weiss behavior only some distance above T_m , which corresponds to the frequency-dependent dielectric maximum. The dashed line is fitting to the Curie-Weiss equation, $\epsilon'(T) = C/(T-T_0)$, with $C = 2.2 \times 10^5$ K and $T_0 = 406$ K. Noticeable deviation from the Curie-Weiss law begins near 445 K. We consider 445 K to be the Burns temperature

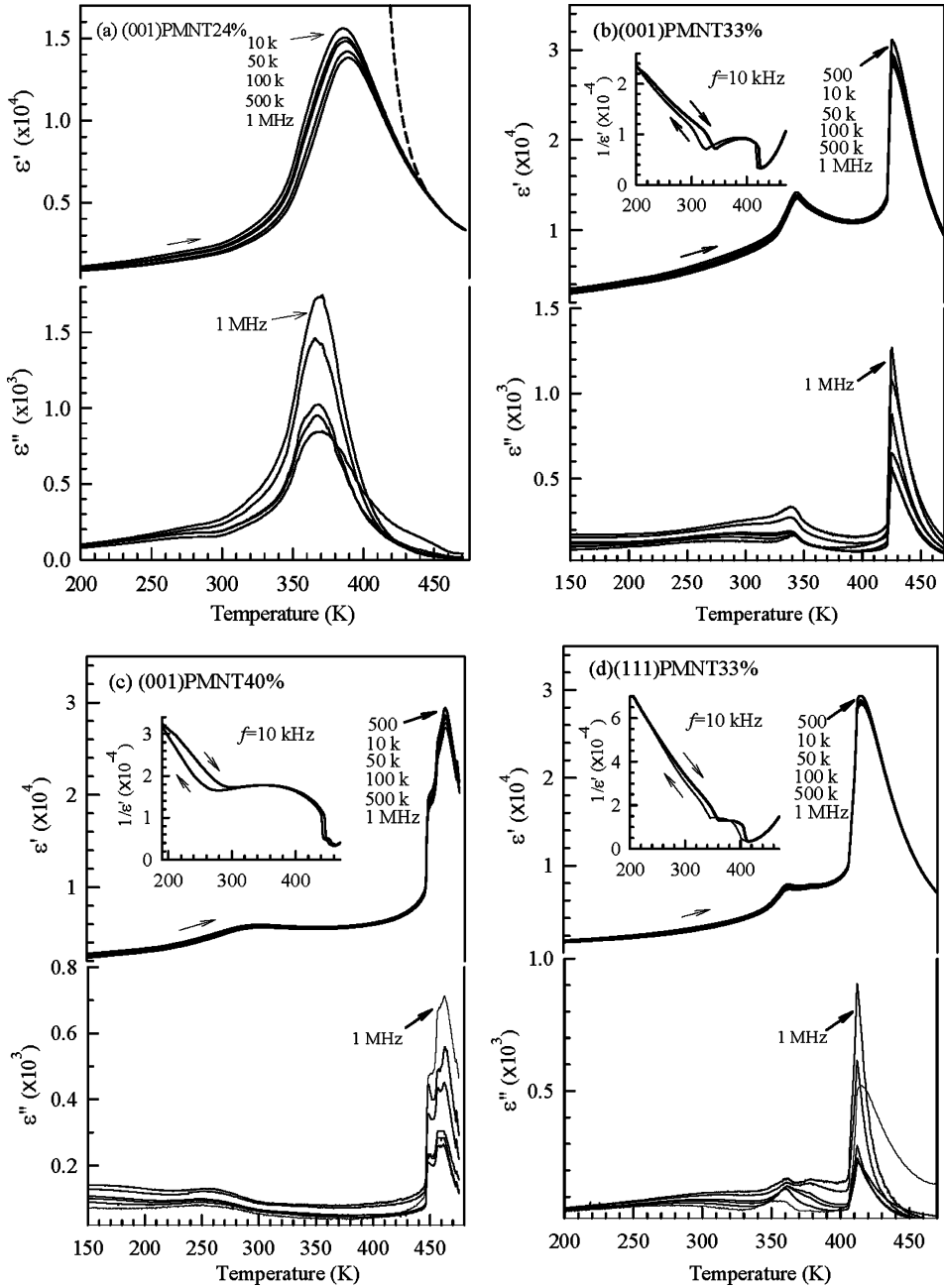


Figure 3. Temperature-dependent and frequency-dependent dielectric permittivity measured in poled (a) (001)PMNT-24%, (b) (001)PMNT-33%, (c) (001)PMNT-40%, and (d) (111)PMNT-33% crystal.

(T_B), below which polar nanoclusters start to develop. Their weaker dielectric response causes deviations from the Curie-Weiss behavior and their dynamics is responsible for the broad dielectric relaxation behavior [16].

Figure 3b shows the temperature-dependent real part ϵ' and imaginary part ϵ'' of dielectric permittivity at measuring frequency $f = 10$ kHz from ZFH for (001)PMNT-33%. Obvious thermal hysteresis is observed near 250–400 K and 415–430 K, respectively. Two steep dips in the reciprocal of ϵ' are seen at 340 (320 K) and 425 (420 K) for ZFH (ZFC), as shown in the inset of Fig. 3b. Both steep phenomena and thermal hysteresis imply two first-order-type transitions near 340 K (320 K) and 425 K (420 K) respectively upon heating (cooling) [17]. The temperature (T_m), which corresponds to dielectric maximum in ZFH and ZFC occurs at 425 and 420 K, respectively. The T_m doesn't show apparent frequency-dependent behavior. Compared with (001) PMNT-24%, (001) PMNT-33% doesn't exhibit clear frequency-dependent relaxation behavior even in the low temperature region, indicating that (001) PMNT-33% has a longer range ordered state.

Figure 3c shows temperature-dependent ϵ' and ϵ'' at several frequencies obtained from ZFH for (001) PMNT-40%. Two thermal hysteresises are observed in the temperature regions of ~ 200 –280 K and ~ 420 –460 K, indicating two first-order-type phase transitions. As shown in the reciprocal of ϵ' , one steep dip near 460 K also confirms a first-order-type transition. The shoulder seen near 450 K most likely is due to phase segregation.

Figure 3d shows temperature-dependent ϵ' and ϵ'' at several frequencies obtained from ZFH for (111) PMNT-33%. Two thermal hysteresises are observed in the temperature regions near 240–360 K and 380–420 K, indicating two first-order-type phase transitions. As shown in the reciprocal of ϵ' , two steep dips near 360 (340 K) and 420 (415 K) upon heating (cooling) also confirm two first-order-type transitions. Compared with (001) PMNT-24%, both (111) and (001) PMNT33% do not exhibit apparent frequency-dependent relaxation behavior.

What are the temperature-dependent phase transitions in the PMNT-x crystals? How are the crystal phases determined? The details of results and discussion regarding phase (structural) transitions determined by the methods of dielectric and polarizing microscopy measurements for the four crystals can be found in Refs. [10, 11], [7, 12], [13], and [14] for (111) PMNT-33%, (001) PMNT-24%, (001) PMNT-40%, and (001) PMNT-33%, respectively. Here, we present the results and discussion of polarizing microscopy for the (001)PMNT-33% crystal, which is the compound near the MPB, as an example to illustrate the methods we have employed to investigate phase (structural) transitions in all four crystals. In addition, we show comparisons for the four crystals.

Thermally Induced Phase Transitions

Figure 4 shows domain micrographs taken with various P/A angle from 0° to 90° at three temperatures, i.e. RT (= 298 K), 350 K, and 430 K for the unpoled (001) PMNT-33% crystal. The domain micrograph taken at P/A: 0° appears the same as that taken at P/A: 90° . As shown in Fig. 4a, the domain matrix at RT (298 K) mostly exhibits extinction at P/A = 0° with respect to the $\langle 110 \rangle$ direction, indicating an R phase. If O or T phase domains exist, there will be also extinction at P/A: 45° . However, no extinction was observed at P/A: 45° . Near 350 K, the domain matrix shows a change, which is consistent with the dielectric anomalies in Fig. 3b. Some stripe-like domains display total extinction at all P/A angle indicating a [001] tetragonal (T_{001}) phase. The M phase domains of the crystal at the corners, as indicated with arrows in Fig. 4b, exhibit extinctions in the ranges of 10 – 15°

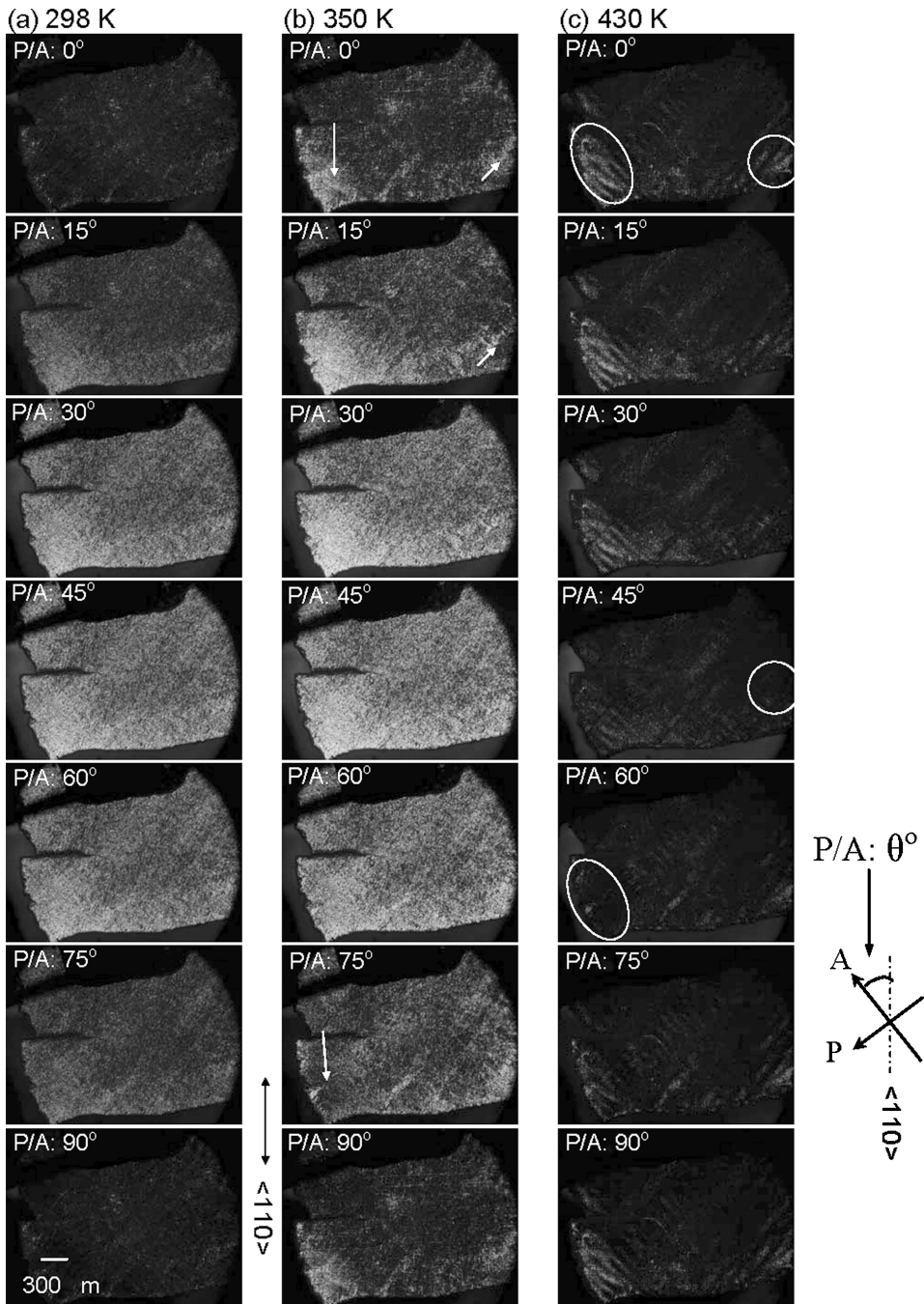


Figure 4. Domain micrographs taken with P/A angles from 0° to 90° at (a) 298 K (RT), (b) 350 K, and (c) 430 K. The graph at the right hand side demonstrates the angle of the crossed analyzer (A) and polarizer (P) pair (i.e. $P/A: \theta^\circ$) measured with regards to the sample's $\langle 110 \rangle$ edge.

and 75–80°. The crystal has coexistence of a dominant R and minor M phase domains, i.e. R(M). As temperature increases further, the domain area and the range of extinction angle for the M phase expand, and the T_{001} phase domains also expand. Near 430 K, the C phase begins to appear as stripes with a total extinction at every P/A angle besides the T_{001} phase domains. In addition, a small portion of the domain matrix exhibits extinction angles of 55–75° and 30–50° as circled in Fig. 4c, indicating the M phase. Near 433 K, the whole crystal becomes C phase. In brief, an $R \rightarrow R(M) \rightarrow R/M/T_{001} \rightarrow C$ phase transition sequence takes place near 343, 350 and 430 K upon heating, respectively. R/M/ T_{001} indicates the coexistence of R, M, and T_{001} phase domains.

***E* Field-Induced Phase Transition**

Figure 5 shows the E field-dependent domain structures taken at RT for three E field strengths while a dc E field was applied along [001]. At $E = 0$ kV/cm, the domain matrix exhibits an R phase with extinction at P/A:0° as shown in Fig. 4a. The domain matrix does not change apparently until 4.1–4.8 kV/cm as shown in Fig. 5a. The domain matrix mostly still retains R phase, but T_{001} and M/T phases are induced near the cracking area, as indicated by an arrow in Fig. 5a, and exhibit extinctions at every P/A angle and in the range of 15–65°, respectively. M/T represents the coexistence of M and T phases with more M phase than T phase domains. Note that the coercive field E_C for the (001) PMNT-33% crystal is about 3 kV/cm as given in Fig. 5d. As the field increases to 11 kV/cm (Fig. 5b), the T_{001} phase domain significantly expands as crossed stripes along [100] and [010] from the cracking area. Some of the R phase domains have also transformed to M and T phase with various nonzero-degree extinction angles, such as 5–15°, 20–50°, and 50–75°. But small portion of the domain matrix circled in Fig. 5b still remains in the R phase. With increasing E field, this E field-induced transition is continuously evidenced by the expansion of the T_{001} phase domain shown as black area of the domain matrix. At $E = 34$ kV/cm, most of the domain matrix becomes macroscopic T_{001} phase domain except for some small R, T, and M phase domains with extinction angles of 0°, 45°, and ~15–45° as shown in Fig. 5c. In addition, a few domains exhibiting no extinction at any P/A angle are embedded in the T_{001} domain matrix, perhaps due to crystal defects and local strain caused by underlying M phase distortions with various different orientations. In brief, the E field-induced phase transition sequences at RT in (001) PMNT-33% include $R \rightarrow T_{001}$, $R \rightarrow M \rightarrow T_{001}$, $R \rightarrow T \rightarrow T_{001}$, and $R \rightarrow M \rightarrow T \rightarrow T_{001}$.

As shown in Fig. 6b, the (001) PMNT-33% crystal cannot completely reach a T_{001} monodomain at $E = 34$ kV/cm applied along [001] at RT [14]. However, the (111) PMNT-33% crystal (Fig. 6d) gradually reaches an R_{111} monodomain at $E = 12$ kV/cm applied along [111] at RT [11]. The (001) PMNT-40% crystal shown in Fig. 6c becomes entirely T_{001} monodomain under $E = 33$ kV/cm applied along [001] [13]. But the (001) PMNT-24% crystal (Fig. 6a) cannot reach a T_{001} monodomain under $E = 44$ kV/cm applied along [001] at RT [12]. Therefore, a monodomain with the orientation along the poling field was not always obtained under the maximum E -field strength in every crystal at RT as expected, such as the (001) PMNT-24% and (001) PMNT-33% with E field applied along [001] [12, 14]. The E field-induced monodomain can be achieved in the PMNT crystals if the dc poling field is along the polar axes of the phase favored by the temperature, such as the (111)PMNT-33% and (001)PMNT-40% crystals [11, 13]. As shown in Fig. 6c, T polar directions are favored at RT in the (001) PMNT-40% so that less E -field poling strength is needed to induce the T phase domains with the field applied along [001]. On the other

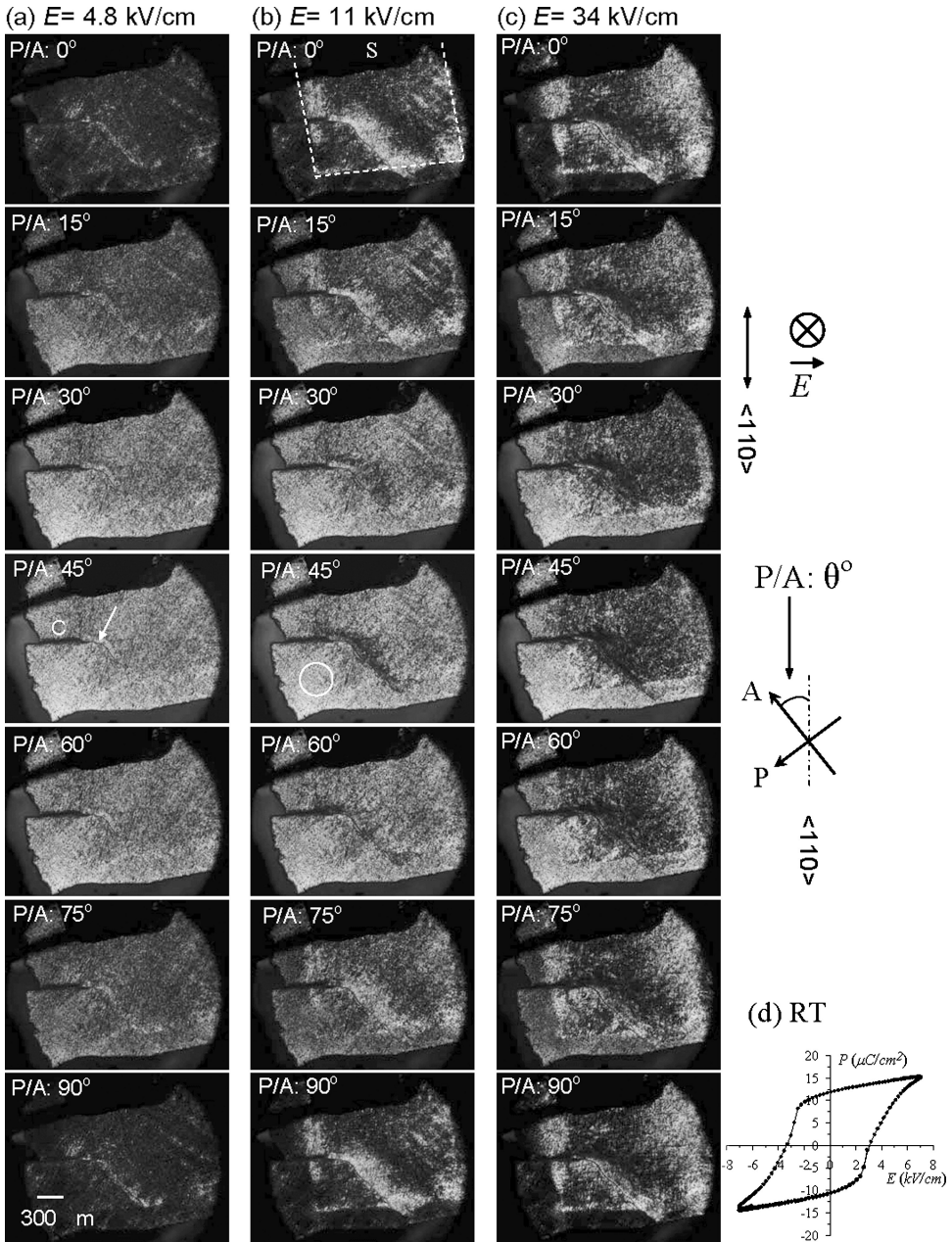


Figure 5. Domain micrographs taken with P/A angle from 0° to 90° at RT under the E field strengths of (a) 4.8 kV/cm, (b) 11 kV/cm, and (c) 34 kV/cm applied perpendicular to the paper. The boundaries of ITO electrodes are indicated by the dash lines. “S” indicates silver paste. (d) hysteresis loops of polarization vs. E field measured at RT in (001)PMNT33% crystal.

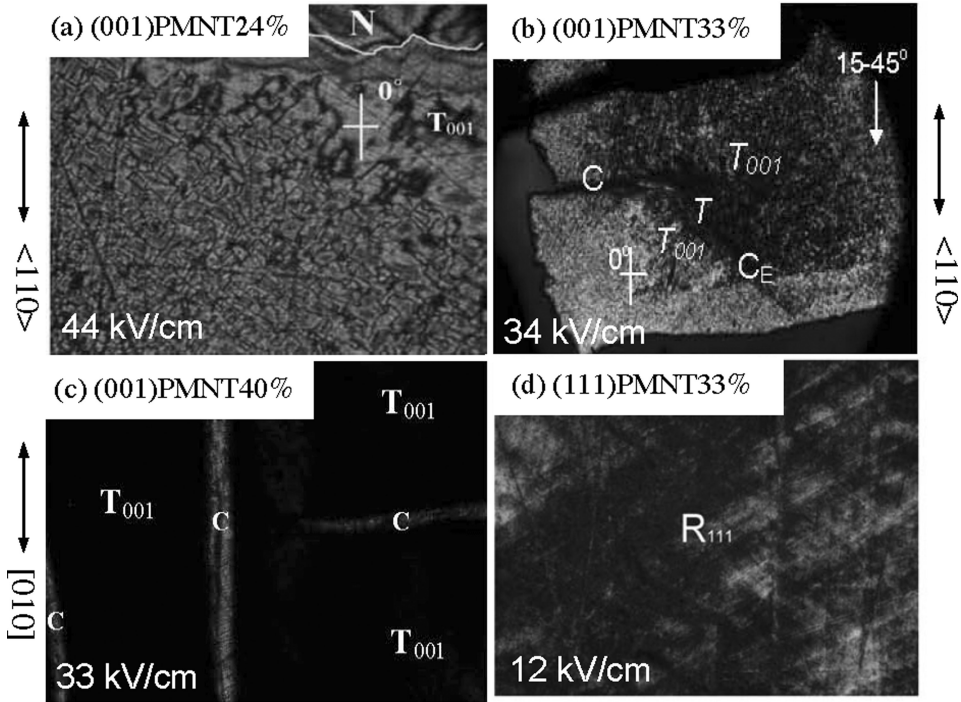


Figure 6. Domain micrographs taken with P/A: 45° at RT under the maximum E field applied perpendicular to the crystal cut planes, including [001] for (001)-cut (a) PMNT-24%, (b) PMNT-33% and (c) PMNT-40% crystals, and [111] for (d) (111)-cut PMNT-33% crystal. “N” is the domain region without ITO electrode. “C” in (c) and “C_E” in (b) are cracks due to E -field poling. “C” in (b) is a crack caused by the polishing process. “T₁₀₀” and “R₁₁₁” indicate [100] tetragonal and [111] rhombohedral domains, respectively. The angles indicated in (a) and (b) are the extinction angles in the corresponding domain regions.

hand, T phase is not favored at RT in the (001) PMNT-24% so that it takes higher E field poling strength to induce the T phase domains.

In the (001) PMNT-24% crystal, an $R \rightarrow T_{001}$ phase transition is induced near $E = 4$ kV/cm through M_A phase domains as E field increases along [001] at RT, i.e. $R \rightarrow M_A \rightarrow T_{001}$ [12]. In the (001)PMNT-40% crystal, the T_{001} phase domains are induced near $E = 11$ kV/cm at RT by the process of polarization rotation of $T \rightarrow M \rightarrow T_{001}$, and this T_{001} phase expands through the whole crystal as the E field increases further [13]. Similarly, in the (001) PMNT-33% crystal the T_{001} phase domains are induced near $E = 4.1$ kV/cm at RT and expand significantly at $E = 11$ kV/cm by various phase transition sequences $R \rightarrow T_{001}$, $R \rightarrow M \rightarrow T_{001}$, $R \rightarrow T \rightarrow T_{001}$, and $R \rightarrow M \rightarrow T \rightarrow T_{001}$ [14].

Conclusions

The intermediate M phases play an essential role in bridging higher symmetries while the E -field and/or temperature induced transitions are taking place in the PMNT- x crystals. In addition, whether or not a single domain (or monodomain) can be induced by a dc E field strongly depends on crystallographic orientation, PT content, and temperature

region where an external dc E field was applied. A monodomain was achieved in the (111) PMNT-33% and (001) PMNT40% while a dc E -field was applied along [001] and [111], respectively. Compared with PMNT-33% and 40%, the (001) PMNT-24% crystal exhibits frequency-dependent relaxation behavior in a wide temperature region and its high-temperature dielectric permittivity shows deviation from the Curie-Weiss law, indicating that dynamics of polar nanoclusters plays an important role in its temperature-dependent phenomena.

Acknowledgments

The authors would like to express sincere thanks to Dr. H. Luo for the crystals. This work was supported by DoD EPSCoR Grant No. N00014-02-1-0657 and NSC Grant No. 94-2112-M-030-004.

References

1. S.-E. Park and T. R. Shrout, Ultrahigh strain and piezoelectric behavior in relaxor based ferroelectric single crystals. *J. Appl. Phys.* **82**, 1804–1811 (1997).
2. S.-E. Park and E. Hackenberger, High performance single crystal piezoelectrics applications and issues. *Curr. Opin. Solid State Mater. Sci.* **6**, 11–18 (2002).
3. P. Han, W. Yan, J. Tian, H. Huang, and H. Pan, Cut directions for the optimization of piezoelectric coefficients of lead magnesium niobate-lead titanate ferroelectric crystals. *Appl. Phys. Lett.* **86**, 052902 (2005) (3 pages).
4. B. Noheda, Structure and high-piezoelectricity in lead oxide solid solutions. *Curr. Opin. Solid State Mater. Sci.* **6**, 27–34 (2002).
5. I.-K. Jeong, T. W. Darling, J. K. Lee, Th. Proffen, R. H. Heffner, J. S. Park, K. S. Hong, W. Dmowski, and T. Egami, Direct Observation of the formation of polar nanoregions in $\text{Pb}(\text{Mg}_{1/3}\text{Nb}_{2/3})\text{O}_3$ using neutron pair distribution function analysis. *Phys. Rev. Lett.* **94**, 147602 (2005) (3 pages).
6. H. Fu and R. E. Cohen, Polarization rotation mechanism for ultrahigh electromechanical response in single-crystal piezoelectrics. *Nature* **403**, 281–283 (2000).
7. C.-S. Tu, R. R. Chien, F.-T. Wang, V. H. Schmidt, and P. Han, Phase stability after an electric-field poling in $\text{Pb}(\text{Mg}_{1/3}\text{Nb}_{2/3})_{1-x}\text{Ti}_x\text{O}_3$ crystals. *Phys. Rev. B.* **70**, 220103 (2004) (4 pages).
8. Z. Feng, X. Zhao, and H. Luo, Composition and orientation dependence of phase configuration and dielectric constant tunability in poled $\text{Pb}(\text{Mg}_{1/3}\text{Nb}_{2/3})\text{O}_3$ - PbTiO_3 single crystals. *J. Physics: Condens. Matter.* **16**, 6771–6778 (2004).
9. M. Davis, D. Damjanovic, and N. Setter, Electric-field-, temperature-, and stress-induced phase transitions in relaxor ferroelectric single crystals. *Phys. Rev. B.* **73**, 014115 (2006) (16 pages).
10. C.-S. Tu, V. H. Schmidt, I.-C. Shih, and R. Chien, Phase transformation via a monoclinic phase in relaxor-based ferroelectric crystal $(\text{PbMg}_{1/3}\text{Nb}_{2/3}\text{O}_3)_{1-x}(\text{PbTiO}_3)_x$. *Phys. Rev. B.* **67** (R), 020102 (2003) (4 pages).
11. C.-S. Tu, V. H. Schmidt, R. Chien, and I.-C. Shih, E -field-induced polarization rotation in $(\text{PbMg}_{1/3}\text{Nb}_{2/3}\text{O}_3)_{1-x}(\text{PbTiO}_3)_x$ crystal. *Appl. Phys. Lett.* **83**, 1833–1835 (2003).
12. R. R. Chien, V. H. Schmidt, C.-S. Tu, L.-W. Hung, and H. Luo, Field-induced polarization rotation in (001)-cut $\text{Pb}(\text{Mg}_{1/3}\text{Nb}_{2/3})_{0.76}\text{Ti}_{0.24}\text{O}_3$. *Phys. Rev. B.* **69**, 172101 (2004).
13. R. R. Chien, V. H. Schmidt, L.-W. Hung, and C.-S. Tu, Temperature- and electric-field-dependent domain structures and phase transformations in (001)-cut tetragonal $\text{Pb}(\text{Mg}_{1/3}\text{Nb}_{2/3})_{1-x}\text{Ti}_x\text{O}_3$ ($x = 0.40$) single crystal. *J. Appl. Phys.* **97**, 114112 (2005) (4 pages).
14. R. R. Chien, C.-S. Tu, V. H. Schmidt, and F.-T. Wang, Electric-field- and temperature-induced phase transitions in high-strain ferroelectric $\text{Pb}(\text{Mg}_{1/3}\text{Nb}_{2/3})_{0.67}\text{Ti}_{0.33}\text{O}_3$ single crystal. *J. Phys. Condens. Matter.* **18**, 8337–8344 (2006).

15. V. H. Schmidt, R. Chien, I.-C. Shih, and C.-S. Tu, Polarization rotation and monoclinic phase in relaxor ferroelectric PMN-PT crystal. *AIP Conference Proceedings* **677**, 160–167 (2003).
16. D. Viehland, S. J. Jang, L. E. Cross, and M. Wuttig, Deviation from Curie-Weiss behavior in relaxor ferroelectrics. *Phys. Rev. B.* **46**, 8003–8005 (1992).
17. K. Uchino, *Ferroelectric Devices*. New York: Marcel Dekker, Inc. (1962) pp. 38–41.